The investigation of 2D monolayers as potential chelation agents in Alzheimer's disease

Neha Pavuluru[1] and Xuan Luo[2]

[1]**National Graphene Research and Development Center, Springfield, Virginia 22151, USA**
[2]**National Graphene Research and Development Center, Springfield, Virginia 22151, USA**

Corresponding author:
Xuan Luo[1]

Email address: xuan.us@gmail.com

ABSTRACT

In this study, we conducted Density Functional Theory calculations comparing the binding energy of the copper- Amyloid-β complex to the binding energies of potential chelation materials. We used the first-coordination sphere of the truncated high-pH Amyloid-β protein subject to computational limits. Binding energy and charge transfer calculations were evaluated for copper's interaction with potential chelators: monolayer boron nitride, monolayer molybdenum disulfide, and monolayer silicene. Silicene produced the highest binding energies to copper, and the evidence of charge transfer between copper and the monolayer proves that there is a strong ionic bond present. Although our three monolayers did not directly present chelation potential, the absolute differences between the binding energies of the silicene binding sites and the Amyloid-β binding site were minimal proving that further research in silicene chelators may be useful for therapy in Alzheimer's disease.

INTRODUCTION

Alzheimer's disease (AD) is the most common cause of dementia worldwide, with a growing prevalence in older individuals (Zhang et al. (2016)). AD is a neurodegenerative disease that interferes with the synaptic responses in the brain leading to the death of neurons (Zhang et al. (2016); DeKosky and Scheff (1990)). The continuous deterioration of neurons leads to impaired cognitive function and behavior in AD patients, placing a significant socioeconomic toll on both the individual and family members (da Silva Falcão et al. (2016); Riley et al. (2002)). These degenerative changes are frequently attributed to neurofibrillary tangles and tau hyperphosphorylation, two pathological hallmarks of AD (Šimić et al. (2016)). However, the main antagonists in AD are understood to be senile plaques (Jean et al. (2019)).

Senile plaques are a result of Amyloid-Beta (Aβ) protein aggregation (Hatami et al. (2017)). Aβ is a 40-42 amino acid residue peptide cut from the C terminal of the amyloid precursor protein (APP) (Pappolla et al. (1998); Hatami et al. (2017); Lesné et al. (2006)). When cut from the β- and γ-secretases, Aβ misfolds and aggregates into senile plaques (Lesné et al. (2006); Sadigh-Eteghad et al. (2015)). An area of interest in Aβ research is the hypothesis that metal ions interact with segments of Aβ and accelerate its aggregation into senile plaques (Lee et al. (2018); Barnham and Bush (2014)). These metal ions interface with the protein by strengthening the formation of beta pleats (Viles (2012)), as well as by strengthening the hydrophilic interactions between certain amino acids, such as His and Asp, by forming salt bridges (Faller et al. (2013)). Both actions are crucial to the development of Aβ as salt bridges impact the tertiary structure of the protein while beta pleats impact the secondary structure. Previous in-vitro studies have verified this hypothesis by attributing elevated levels of copper, zinc, and iron to increased Aβ aggregation (Adlard and Bush (2018); Tõugu et al. (2011); Mujika et al. (2017)). Although some studies indicate that metal ions play a role in the formation of senile plaques, uncertainties about the presence of metal ions in Aβ aggregation exist and the mechanisms of metal and Aβ interaction remain unclear. To resolve this ambiguity, recent research efforts have emphasized determining the metal-Aβ

binding sites by identifying the coordination point at which the metal ion binds to the amino acid residues (Del Barrio et al. (2017)). Researchers have developed at least three investigational approaches: 1) absorption spectroscopy computational methods; 2), x-ray methods; and first-principles computations (Strodel and Coskuner-Weber (2019)).

Conclusions that were drawn regarding copper coordination to Aβ reveal that it occurs in the Histidine (His) 13 and 14 residues through their nitrogen atoms (Minicozzi et al. (2008b); Curtain et al. (2001); Mutter et al. (2018); Streltsov et al. (2008)) and N-terminal (Hane et al. (2013); Syme et al. (2004); Azimi and Rauk (2011); Rana and Sharma (2019)) along with contribution of one oxygen atom (Rimola et al. (2011)). However, many theories of copper coordination were proposed and inconsistencies exist among the varying propositions. For instance, while some studies support tyrosine involvement in copper coordination through its oxygen atom (Minicozzi et al. (2008a)), other works suggest its irrelevance (Minicozzi et al. (2008a); Kowalik-Jankowska et al. (2003); Karr and Szalai (2007)). Contradicting theories also exist in regards to the coordination sequence between copper and regions among the Aβ peptide. Proposed coordinations include four nitrogen (N4), three nitrogen one oxygen (N3O1), and three nitrogen three oxygen (N3O3) patterns (Rauk (2009)).

The role of metal ions in enhancing Aβ aggregation has also led to the possibility of utilizing them as therapeutic targets to halt the progression of AD (Ayton et al. (2015)). One proposal to combat metal-induced aggregation is chelation therapy. Chelation is the practice of utilizing certain compounds to remove excess metals in the body. Metal chelates such as clioquinol and PBT2 were found to be effective in clinical trials of brain diseases, such as AD and Huntington's Disease (Ayton et al. (2015); Lannfelt et al. (2008)), indicating chelation therapy's potential treatment as a treatment for AD. This has encouraged continued development of derivatives to improve clinical effectiveness and reduce cytotoxic effects. However, these previously explored chelation agents are not suitable for treating AD due to their inability to permeate the blood brain barrier, demonstrate efficient selective targeting, and produce tolerable side effects (Minicozzi et al. (2008a)). To overcome the issues of these metal chelates, recent research has encouraged the use of 2D monolayers as therapeutic agents for AD, given the ability of their small size will be able to permeate the blood brain barrier, as well as their superior surface area which would be effective for adsorption. However, the concept of utilizing 2D monolayers in treating AD is relatively new. While research in the field of 2D monolayer chelation is sparse, there have been studies where nanoparticles were utilized for drug-delivery and blood-brain-barrier permeation. These nanoparticles have demonstrated promising results when in previous in-vitro studies. For example, both boron nitride nanotubes and molybdenum disulfide nanoparticles have been used in the treatment of brain diseases (Ciofani et al. (2011); Han et al. (2017)), and recent clinical trials have also found that silica based materials may reduce cognitive impairment associated with AD (Davenward et al. (2013)). Based on this information, we selected three biocompatible monolayers and tested their chelation potential.

In order to make accurate predictions about the interactions between metal ions, 2D nanomaterials, and amino acids, computational platforms, such as theoretical quantum biological and quantum chemical studies, are important in this field (Gomez-Castro et al. (2014); Marino et al. (2010); Drew et al. (2009); Mantsyzov et al. (2018)). One of the important concepts in these calculations is binding energy. Binding energy evaluated from total energy calculations can be used to identify structural relationships between metal ions and Aβ as well as the efficiency of potential chelation treatments. This study will focus on the interactions between copper and the truncated Aβ residue along with boron nitride, molybdenum disulfide, and silicene. Analysis of these effects may be useful towards mitigation of AD as well as exploration of new methods of disease treatment. In this study, we report the specific computational methods used, our results, and direct interpretations of the calculations. We also discuss our findings, as well as the future work to be completed in order to supplement our findings.

METHOD

In this study, we performed Density Functional Theory (DFT) calculations with the Generalized Gradient Approximation (GGA) (Blöchl (1994)) pseudopotentials in the form of Perdew-Burke-Ernzerhof (PBE) (Perdew et al. (1996)) implemented in the ABINIT (Gonze et al. (2009, 2005)) code. We used the Projected Augmented Wave (PAW) method to generate the pseudopotentials used. The electron configurations and the radius cutoffs used to generate these PAW pseudopotentials are listed in Table I.

Table 1. *Electron Configurations and Radius Cutoff of Each Element for Generating the PAW Pseudopotentials Used in the Current Study*

Element	Electron Configurations	Radius Cut-Off (Bohr)
Copper (Cu)	[Ne] $3s^2\ 3p^6\ 4s^1\ 3d^{10}$	2.02
Boron (B)	[He] $2s^2\ 2p^1$	1.70
Nitrogen (N)	[He] $2s^2\ 2p^3$	1.20
Carbon (C)	[He] $2s^2\ 2p^2$	1.51
Oxygen (O)	[He] $2s^2\ 2p^4$	1.41
Hydrogen (H)	$1s^1$	1.00
Molybdenum (Mo)	[Kr] $4d^5\ 5s^1$	2.20
Sulfur (S)	[Ne] $3s^2\ 3p^4$	1.92
Silicon (Si)	[Ne] $3s^2\ 3p^2$	1.91

0.1 Convergence Calculations

The main calculation that will be conducted in this study is binding energy. In order to find the binding energy, however, the total energy of the materials must be known. Total energy can be determined from a series of calculations which involve finding the kinetic energy cutoff, the K-Mesh, the optimized lattice parameters, and the vacuum height. Convergence calculations were accomplished using the self-consistent field method. Values were converged until the difference in total forces for two consecutive datasets was less than 1×10^{-4} Ha/Bohr. Lattice parameter relaxation was done using the Broyden-Fletcher-Goldfarb-Shanno (BFGS) method in order to find the optimized lattice parameters. These calculations continued until the maximum forces converged to less than 5×10^{-4} Ha/Bohr. Using these converged values, the total energy can be found. The total energy calculations were carried out using the converged parameters until the difference in total energy in the self-consistent field cycles was less than 1×10^{-10} Ha/Bohr.

0.2 Materials

0.2.1 Copper and 2D Monolayer Calculations

Convergence of kinetic energy cut-off was calculated for the copper-ion investigated in this work. This was accomplished using the convergence calculations described above. The kinetic energy cut-off was determined to be 22 Ha.

The 2D materials analyzed in this work include boron nitride, molybdenum disulfide, and silicene. Convergence studies were performed for kinetic energy cutoff, vacuum space, and K-Mesh. Converged values were then utilized for relaxation of the atomic structure and unit cell dimensions. These calculations were performed using the 1×1 unit cell. The converged values are presented in Table II.

Table 2. *Converged Kinetic Energy Cut-Off, k-mesh, and vacuum of 2D materials*

Material	Kinetic Energy Cutoff (Ha)	K-Mesh	Vacuum (Bohr)
Boron Nitride	24	$6\times6\times1$	13
Silicene	13	$12\times12\times1$	18
Molybdenum Disulfide	20	$10\times10\times1$	30

0.2.2 Copper Interaction with Aβ

Since the study involves the first coordination sphere of the protein, the truncated Aβ was used in the copper-Aβ calculations. These calculations were carried out in a high-pH environment characterized by a pH of 8. A high-pH environment was used as previous literature determined that Aβ produces higher binding energies in this environment(Alí-Torres et al. (2014)). The first coordination binding site of the high-pH Aβ consisted of His6, His13, His14, and Ala2. Ambiguous sequences beyond the direct binding at the first coordination sphere were saturated with hydrogen atoms. For accommodation of computational limitations, His ligands were modeled by their 4-methylimidazole ($C_3H_4N_2$) side chains, the N-terminal by NH_2 , and the alanine side chain was modelled by an OH group. As seen in Figure 2, the copper-ion lies at the central location surrounded by the components of the protein.

Initial first coordination sphere complexes were constructed and optimized in the Jmol software. The optimized coordinates of the structure were then exported and used in relaxation calculations. The complex was relaxed, and optimized geometries were used to calculate the total energy of the complex, both with and without coordination to the copper-ion.

Total energy calculations were then run for successful configurations: for the total interface, the isolated copper molecule, and the isolated surface. Binding energy was defined by

$$E_{binding} = E_{substrate+metal} - E_{metal} - E_{substrate} \tag{1}$$

where $E_{binding}$ represents the binding energy, $E_{metal+substrate}$ is the total energy of the metal-substrate complex, $E_{substrate}$ is the total energy of the substrate, and E_{metal} is the total energy of the individual metal ion. Higher magnitudes are associated with higher affinities.

0.2.3 Copper Interaction with 2D Monolayers

Copper interactions with 2D materials were accomplished using a 2×2 supercell. The vacuum was the same as that converged using the 1×1 unit cell. Out of the determined kinetic energy cutoffs of copper and the 2D materials, the higher kinetic energy cutoff was chosen for the 2×2 supercell. The k-mesh was halved, and the unit cell dimension doubled. Copper-ion coordination was observed at three binding locations to determine the most optimal binding site. The binding locations consisted of the top of the atoms, the hollow of the surface, and the bridge site. Total energy calculations were carried out for the copper-ion, the 2D material, and the copper-2D complex. Potential chelation candidates were determined by comparing the binding energies of the copper-ion and 2D materials to the binding energy of the copper-ion and the Aβ structure.

Furthermore, charge density values were evaluated by using this equation

$$\Delta\rho = -\frac{1}{2}(\rho_{metal+substrate} - \rho_{metal} - \rho_{substrate}) \tag{2}$$

where $\Delta\rho$ represents the charge transfer between the metal and the substrate, $\rho_{metal+substrate}$ represents the charge of the metal-substrate complex, ρ_{metal} represents the charge of the individual metal ion, $\rho_{substrate}$ is charge of the individual substrate. Isosurface values were determined to display the charge densities at select viewing sites. Positive isosurface values represent loss of electrons, and negative isosurface values represent the gain of electrons.

1 RESULTS

In this section, we report our results on the binding strength between the copper-ion and selected substrates (the truncated high-pH Aβ subject to computational limits, as well as the 2D monolayers). Referring to Equation 1, binding energies were calculated through relating the total energies of the copper-ion, the substrate, and the copper-substrate complex. These binding energies were used to further analyze and interpret the meaning of our results in the context of the issue, or specifically, the chelation potential of the explored treatment materials. The chelation potential of a 2D monolayer is determined by comparing the binding energy of the copper-2D material complex and the binding energy of the copper-Aβ complex subject to computational limits. If the binding energy of the copper-2D material complex is greater than the binding energy of the copper-Aβ complex, then the 2D material possesses adequate chelation potential. Charge transfer was also plotted using Equation 2 to determine the strengths of the bonds between copper and the monolayers.

1.1 Pristine Copper and 2D Monolayers

The optimized lattice parameters calculated in this study as well as the experimental lattice parameters from previous studies are listed in Table III(Bean and McKenna (2016); Wang et al. (2017); Molina-Sanchez and Wirtz (2011); Pflugradt et al. (2014)) and the visualizations of the 2D Monolayers can be seen in Figure 1. Based on the table, we can see that the lattice parameters obtained in this study closely resemble the experimental values.

Table 3. *Optimized Lattice Parameters and Experimental Lattice Parameters of the Bulk Metals and Pristine 2D Monolayers*

Material	Current (Bohr)	Experimental (Bohr)	% Error
Copper	6.74	6.79Bean and McKenna (2016)	0.7364
Boron Nitride	4.75	4.73Wang et al. (2017)	0.4228
Molybdenum Disulfide	5.98	5.91Molina-Sanchez and Wirtz (2011)	0.4228
Silicene	7.23	7.29Pflugradt et al. (2014)	0.8230

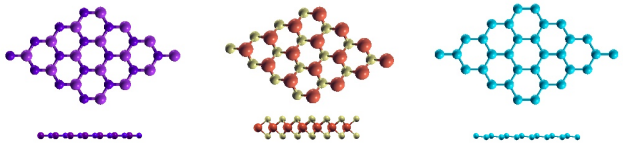

(a) (b) (c)

Figure 1. *The visualizations of the top and side views of the relaxed monolayers (a) boron nitride, (b) molybdenum disulfide, (c) silicene. In these structures, boron is represented by purple, nitrogen by dark blue, sulfur by yellow, molybdenum by orange, and silicon by light blue.*

1.2 Copper Interaction with Aβ

The calculation regarding copper-ion and the high-pH Aβ subject to computational limits was carried out using the N3O1 sequence of the first-coordination sphere. The high-pH coordination sphere, which represents a pH of 8, consisted of 3 His ligands and an oxygen atom. Relaxation calculations were done for the complex in a large box and the optimized lattice parameters and atomic coordinates were used to find the total energy.

The optimized geometry of the copper-ion coordination to high-pH coordination sphere is visualized in Figure 2 and the binding energy is presented in Table IV.

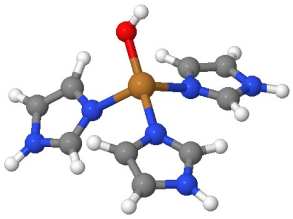

Figure 2. *Fully relaxed copper-ion and high-pH Aβ complex. For the Aβ ligand, carbon is represented by grey, hydrogen by white, nitrogen by blue, and oxygen by red. Copper is represented by brown.*

Table 4. *Binding energy for the high-pH Aβ copper-ion complex*

Element	$E_{high-pH}$ (Ha)
Copper	-0.7262

1.3 Copper Interaction with 2D Monolayers

Because of copper's high affinity towards both the low-pH and high-pH structures of the Aβ protein, we proceeded to investigate its attraction towards the different 2D monolayers. Total energy investigations of atom absorption to boron nitride, MoS_2, and silicene along with calculated binding energies are presented in Table V, VI, and VII, respectively. Based on Equation 1, the binding energies between copper and these monolayers should be negative. Negative binding energies that are large in magnitude indicate that copper and the monolayer have formed a strong bond and a stable structure. Moreover, referring to Equation 2, the presence of charge transfer is also an indicator of increased bond strength.

1.3.1 Copper-Boron Nitride

Copper coordination to boron nitride was performed using a 2×2 supercell with a kinetic energy cutoff of 24 Ha. Four binding locations (the top of the boron atom, the top of the nitrogen atom, the hollow of the monolayer, and the bridge site) were used to determine the most optimal binding site. All four of these binding locations demonstrated different binding affinities, and copper revealed a preference for the top of the boron atom. When copper is placed on top of the boron atom, this results in a binding energy of -0.5027 Ha which means that copper forms a stable structure with boron nitride. The site with the lowest binding affinity was the hollow site with a binding energy of -0.4419 Ha. Although less stable than the top of the boron atom, this binding site still results in a negative binding energy which shows that it forms a somewhat stable bond with the monolayer. Visualizations of the binding sites of boron nitride and copper as well as their charge transfers are shown in Figure 3. The binding energies are shown in Table V.

Table 5. *Binding Energies (Ha) for Copper Absorbed onto Boron Nitride. Cu^H , Cu^{TB} , Cu^{TN}, and Cu^B are representative of copper coordination to the center, top of the boron, top of the nitrogen, and bridge locations respectively*

Boron Nitride Copper Binding Configuration	$E_{binding}$ (Ha)
Cu^H	-0.4419
Cu^{TB}	-0.5027
Cu^{TN}	-0.5027
Cu^B	-0.5027

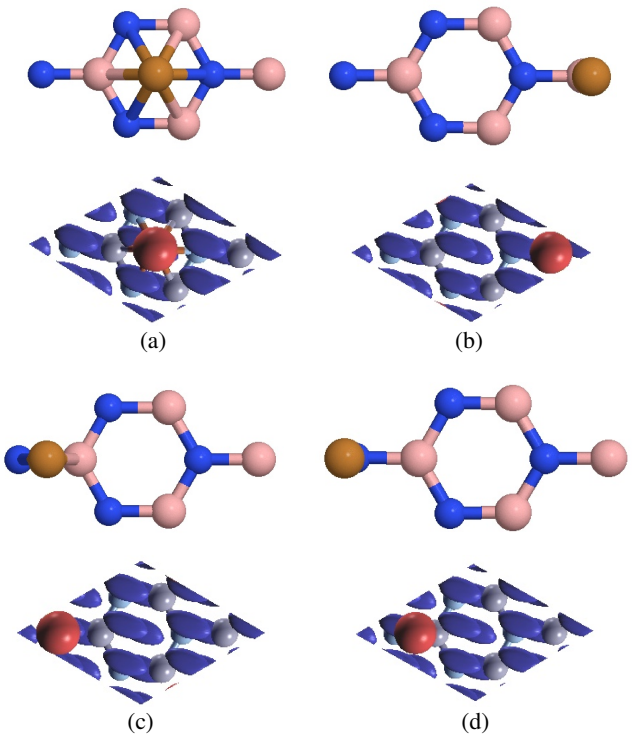

Figure 3. *The atomic structures of copper coordination to boron nitride followed by the charge transfers below. (a) The hollow of boron nitride, (b) The top of boron, (c) The top of nitrogen, and (d) The bridge site. For the atomic structures, the boron atoms are represented by pink, the nitrogen atoms by blue, and the copper atoms by brown. For the charge transfer, red shows the gain of negative charge, whereas blue shows the loss of negative charge. The isosurface value used was +/- 0.03 e/Bohr^3*

1.3.2 Copper-MoS_2

Similar to the copper and boron nitride calculations, copper coordination to MoS_2 was performed using a 2×2 supercell with a kinetic energy cutoff of 22 Ha. Three binding locations (the top of the Mo atom, the top of the S atom, and the hollow of the monolayer) were used to determine the most optimal binding site. Copper revealed a preference for the top of the Mo atom with a binding energy of -0.5417 Ha, which means that it forms a stable bond with the Mo atom. The site with the lowest binding affinity was the top of the S atom which had a binding energy of -0.5270 Ha. Although this binding energy is still negative, it is lower compared to the other binding sites and results in the least stable copper-MoS_2 structure. Visualizations of the binding sites of MoS_2 and copper and their charge transfers are shown in Figure 4. The binding energies are listed in Table VI.

Table 6. *Binding Energies (Ha) for Copper Absorbed onto the MoS_2 Surface. Cu^H, Cu^{TM}, and Cu^{TS} are representative of copper coordination to the center, top of the Mo atom, and top of the S atom, respectively*

MoS_2 Copper Binding Configuration	$E_{binding}$ (Ha)
Cu^H	-0.5368
Cu^{TM}	-0.5417
Cu^{TS}	-0.5270

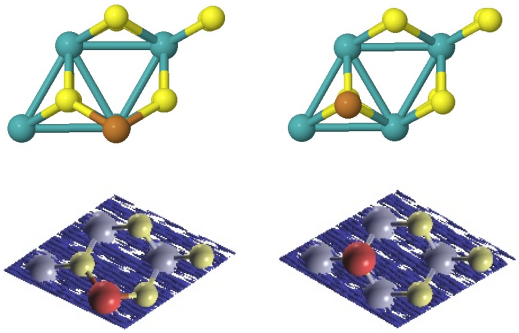

(a) (b)

Figure 4. *The atomic structures of copper coordination to MoS_2 followed by the charge transfers below. (a) The top of the Mo atom and (b) The top of the S atom. For the atomic structures, the molybdenum atoms are represented by light blue, the sulfur atoms by yellow, and the copper atoms by brown. For the charge transfer, red shows the gain of negative charge, whereas blue shows the loss of negative charge. The isosurface value used was +/- 0.03 e/Bohr^3*

1.3.3 Copper-Silicene

We also investigated copper coordination to the silicene surface using a 2×2 supercell, consistent with the previous calculations, and a kinetic energy cutoff of 22 Ha. We used three binding sites (the top of the Si atom, the hollow of the monolayer, and the bridge site) to find the most optimal binding site for silicene. Copper revealed a preference for the hollow site with a binding energy of -0.6298 Ha. This binding energy is the highest in magnitude compared to all of the copper-monolayer calculations which indicates that copper and the hollow of silicene form the most stable structure. The site with the lowest binding affinity was the bridge site with a binding energy of -0.5672 Ha. This binding energy is still significantly higher than some of the other copper-monolayer binding energies proving this configuration to be a relatively stable structure. Visualizations of the binding sites of silicene and copper as well as their charge transfers are shown in Figure 5. The binding energies are presented in Table VII.

Exploring the atomic structures and binding energies of copper to these three monolayers, we can see that copper forms stable structures with these three monolayers. Moreover, the presence of charge transfer between copper and the monolayers indicates that it forms stable bonds. In charge transfer, the copper atom is seen gaining charge, whereas the monolayers are seen losing charge. More specifically, the gaining of charge occurs at the bonds between copper and the monolayer which demonstrates increased bond strength.

Table 7. *Binding Energies (Ha) for Copper Absorbed onto the Silicene Surface. Cu^H, Cu^T, and Cu^B are representative of copper coordination to the center, top of the Si atom, and the bridge site, respectively*

Silicene Copper Binding Configuration	$E_{binding}$ (Ha)
Cu^H	-0.6298
Cu^T	-0.5809
Cu^B	-0.5672

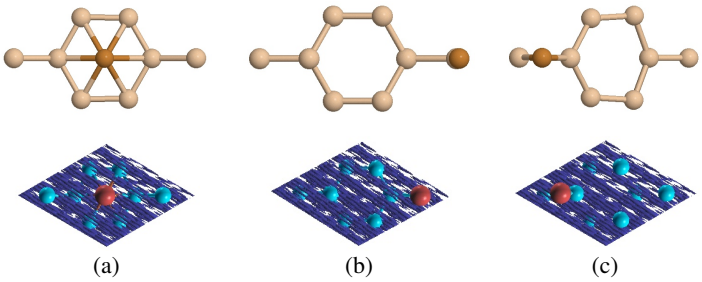

(a) (b) (c)

Figure 5. *Copper coordination to silicene followed by the charge transfers below. (a) The hollow of silicene, (b) The top of Si atom, and (c) The bridge site. For the atomic structures, the silicon atoms are represented by ivory and the copper atoms by brown. For the charge transfer, red shows the gain of negative charge, whereas blue shows the loss of negative charge. The isosurface value used was +/- 0.03 e/Bohr^3*

2 DISCUSSION

After processing our results, we found that while the 2D materials investigated in this study don't directly have potential as metal chelators, their structural features and behavior when binding to copper (especially silicene) can spark further research in the field of AD related metal chelation.

During the course of this study, we investigated the binding of copper to three different materials: boron nitride, molybdenum disulfide, and silicene, to determine chelation potential as defined in the Results section.

Boron nitride was chosen in this study due to its recent applications in biomedical settings. Boron nitride nanotubes have been used in the drug-delivery and treatment of brain diseases (Ciofani et al. (2011)) which makes the boron nitride monolayer a novel device for metal chelation. Moreover, the structure of boron nitride closely resembles graphene which has been proven to have promising results in the treatment of AD. Comparison of binding energies observed for copper coordination to the boron nitride surface at different locations indicated a preference for the top of the boron atom. The binding energy of the copper adsorbed boron nitride structure at the top boron atom configuration, despite demonstrating moderate affinity, was less than the binding energy of the copper-Aβ high-pH complex subject to computational limits, with a value of -0.5027 Ha compared to -0.7262 Ha. However, the absolute difference between the binding energies of the copper-Aβ high-pH complex subject to computational limits and the copper-boron-nitride complex is 0.2235 Ha. This minimal energy difference may prompt further research into boron nitride chelators with slight modifications, such as changes in pressure or temperature in order to develop a more effective material.

Binding energies between copper and molybdenum disulfide, proved similar inabilities towards direct chelation potential. Greatest preference was displayed for the site above the molybdenum atom, most likely due to this position's interaction with the nearby sulfur atoms. However, the binding energy was lower than that of the copper-Aβ complex subject to computational limits, demonstrating this version of the material's inability to directly participate in copper chelation. This could be explained by the stability of molybdenum disulfide, as certain structures of molybdenum disulfide are less stable than others (Dallavalle et al. (2012)). Furthermore, the absolute difference between the binding energies of the copper-Aβ high-pH complex subject to computational limits and the copper-molybdenum-disulfide complex at the top molybdenum atom configuration is 0.1845 Ha, presenting that molybdenum disulfide may have potential as a chelator after slight modifications. Future studies should explore the different

structures of molybdenum disulfide, both trigonal prismatic and octahedral, as well as changes in pressure and temperature in order to yield the ideal monolayer for metal chelation.

Binding energies were also observed for copper coordination to the silicene material. Silicene was initially selected as its high surface area is suitable for metal adsorption, and its buckled structure points towards reactivity that may allow copper binding. Recent clinical trials have also revealed that silica particles may reduce the cognitive impairment associated with AD (Davenward et al. (2013)). Analysis of copper coordination to silicene revealed that copper displayed a preference for the hollow site. However, the binding energy at this site, was less than the copper-Aβ high-pH complex subject to computational limits with a value of -0.6298 Ha compared to -0.7262 Ha. However, the absolute difference between the hollow configuration of silicene and the high-pH copper-Aβ structure subject to computational limits is 0.0964 Ha. This minimal energy difference correlates to the idea that silicene could be further explored in AD therapy. Future works should investigate environmental changes on the binding energies of silicene in order to produce an ideal chelator.

After examining all three 2D monolayers for chelation potentional, we propose that silicene may be a material useful for further research. The minimal absolute energy difference between the copper-Aβ high-pH complex subject to computational limits and the hollow configuration of the copper-silicene complex justify, that with external and internal modifications, silicene may be an effective chelation agent.

3 CONCLUSION

In summary, we performed Density Functional Theory calculations to determine the binding affinity between copper and the high-pH Aβ subject to computational limits. We also calculated the binding affinities between copper, boron nitride, molybdenum disulfide, and silicene to propose adequate materials for chelation therapy.

Binding energy calculations and charge transfer calculations were conducted for the copper-2D monolayer structures. The direct chelation potential of these monolayers was determined by comparing the copper-2D monolayer binding energies to the binding energy of the copper-Aβ complex in a high-pH environment subject to computational limits. Examining our results, we found that the monolayer that produced the highest binding energy was silicene when copper was coordinated to its hollow site. Even though the binding energy was less than the copper-Aβ high-pH complex, the absolute difference between the hollow configuration of silicene and the copper-Aβ structure was 0.0964 Ha, proving that further research into silicene may be a valuable task. The same conclusion applies for boron nitride and molybdenum disulfide as well. Further research into these monolayers as well as the manipulation of internal and external properties may lead to advances for chelation therapy in Alzheimer's disease.

Investigations in this study may contribute to the understanding of chelation therapy as a potential solution to Alzheimer's Disease; however, the platforms implemented in this study are limited to only the first coordination sphere of the Aβ protein. One limitation of the DFT is that the size of the protein is important to capture the segmental stability. This study used one aspect of Aβ's ligand-receptor system in order to compare binding energies. Future explorations in this field may consider the continuation of these computational approaches on the full length Aβ model to allow consideration of physical effects of the rest of the sequence. Moreover, future studies should also take into account the complex environment of the human body, which may affect binding energies. Because the application of 2D materials as chelating agents is a new field in the development of Alzheimer's therapy, many monolayers and their effects on the metals relevant to AD progression are largely unexplored. This study has proposed promising 2D copper chelators that may be useful for future research.

ACKNOWLEDGMENTS

We would like to thank Dr. Geifei Qian for the technical assistance.

REFERENCES

Adlard, P. A. and Bush, A. I. (2018). Metals and alzheimer's disease: how far have we come in the clinic? *Journal of Alzheimer's Disease*, 62(3):1369–1379.

Alí-Torres, J., Mirats, A., Marechal, J.-D., Rodríguez-Santiago, L., and Sodupe, M. (2014). 3d structures and redox potentials of cu2+–aβ (1–16) complexes at different ph: A computational study. *The Journal of Physical Chemistry B*, 118(18):4840–4850.

Ayton, S., Lei, P., and Bush, A. I. (2015). Biometals and their therapeutic implications in alzheimer's disease. *Neurotherapeutics*, 12(1):109–120.

Azimi, S. and Rauk, A. (2011). On the involvement of copper binding to the n-terminus of the amyloid beta peptide of alzheimer's disease: a computational study on model systems. *International Journal of Alzheimer's Disease*, 2011.

Barnham, K. J. and Bush, A. I. (2014). Biological metals and metal-targeting compounds in major neurodegenerative diseases. *Chemical Society Reviews*, 43(19):6727–6749.

Bean, J. J. and McKenna, K. P. (2016). Origin of differences in the excess volume of copper and nickel grain boundaries. *Acta Materialia*, 110:246–257.

Blöchl, P. E. (1994). Projector augmented-wave method. *Physical review B*, 50(24):17953.

Ciofani, G., Danti, S., Ricotti, L., D'Alessandro, D., Moscato, S., Berrettini, S., Mattoli, V., and Menciassi, A. (2011). Boron nitride nanotubes: production, properties, biological interactions and potential applications as therapeutic agents in brain diseases. *Current Nanoscience*, 7(1):94–109.

Curtain, C. C., Ali, F., Volitakis, I., Cherny, R. A., Norton, R. S., Beyreuther, K., Barrow, C. J., Masters, C. L., Bush, A. I., and Barnham, K. J. (2001). Alzheimer's disease amyloid-β binds copper and zinc to generate an allosterically ordered membrane-penetrating structure containing superoxide dismutase-like subunits. *Journal of Biological Chemistry*, 276(23):20466–20473.

da Silva Falcão, D. V., Teodoro, M. L. M., and Bucher-Maluschke, J. S. N. F. (2016). Family cohesion: A study on caregiving daughters of parents with alzheimer's disease. *Interpersona: an International Journal on Personal Relationships*, 10(supp1):61–74.

Dallavalle, M., Sandig, N., and Zerbetto, F. (2012). Stability, dynamics, and lubrication of mos2 platelets and nanotubes. *Langmuir*, 28(19):7393–7400.

Davenward, S., Bentham, P., Wright, J., Crome, P., Job, D., Polwart, A., and Exley, C. (2013). Silicon-rich mineral water as a non-invasive test of the 'aluminum hypothesis' in alzheimer's disease. *Journal of Alzheimer's Disease*, 33(2):423–430.

DeKosky, S. T. and Scheff, S. W. (1990). Synapse loss in frontal cortex biopsies in alzheimer's disease: correlation with cognitive severity. *Annals of Neurology: Official Journal of the American Neurological Association and the Child Neurology Society*, 27(5):457–464.

Del Barrio, M., Borghesani, V., Hureau, C., and Faller, P. (2017). Metal-binding to amyloid-β peptide: Coordination, aggregation, and reactive oxygen species production. In *Biometals in Neurodegenerative Diseases*, pages 265–281. Elsevier.

Drew, S. C., Noble, C. J., Masters, C. L., Hanson, G. R., and Barnham, K. J. (2009). Pleomorphic copper coordination by alzheimer's disease amyloid-β peptide. *Journal of the American Chemical Society*, 131(3):1195–1207.

Faller, P., Hureau, C., and Berthoumieu, O. (2013). Role of metal ions in the self-assembly of the alzheimer's amyloid-β peptide. *Inorganic Chemistry*, 52(21):12193–12206.

Gomez-Castro, C. Z., Vela, A., Quintanar, L., Grande-Aztatzi, R., Mineva, T., and Goursot, A. (2014). Insights into the oxygen-based ligand of the low ph component of the cu2+-amyloid-β complex. *The Journal of Physical Chemistry B*, 118(34):10052–10064.

Gonze, X., Amadon, B., Anglade, P.-M., Beuken, J.-M., Bottin, F., Boulanger, P., Bruneval, F., Caliste, D., Caracas, R., Cote, M., Deutsch, T., Genovese, L., Ghosez, P., Giantomassi, M., Goedecker, S., Hamann, D., Hermet, P., Jollet, F., Jomard, G., Leroux, S., Mancini, M., Mazevet, S., Oliveira, M., Onida, G., Pouillon, Y., Rangel, T., Rignanese, G.-M., Sangalli, D., Shaltaf, R., Torrent, M., Verstraete, M., Zerah, G., and Zwanziger (2009). Abinit: First-principles approach of materials and nanosystem properties. *Computer Physics Communications*, 180:2582–2615.

Gonze, X., Rignanese, G.-M., Verstraete, M., Beuken, J.-M., Pouillon, Y., Caracas, R., Jollet, F., Torrent, M., Zerah, G., Mikami, M., Ghosez, P., Veithen, M., Raty, J.-Y., Olevano, V., Bruneval, F., Reining, L., Godby, R., Onida, G., Hamann, D., and Allan, D. (2005). A brief introduction to the abinit software package. *Zeitschrift für Kristallographie*, 220:558–562.

Han, Q., Cai, S., Yang, L., Wang, X., Qi, C., Yang, R., and Wang, C. (2017). Molybdenum disulfide nanoparticles as multifunctional inhibitors against alzheimer's disease. *ACS Applied Materials & Interfaces*, 9(25):21116–21123.

Hane, F., Tran, G., Attwood, S. J., and Leonenko, Z. (2013). Cu2+ affects amyloid-β (1–42) aggregation by increasing peptide-peptide binding forces. *PloS One*, 8(3):e59005.

Hatami, A., Monjazeb, S., Milton, S., and Glabe, C. G. (2017). Familial alzheimer's disease mutations

within the amyloid precursor protein alter the aggregation and conformation of the amyloid-β peptide. *Journal of Biological Chemistry*, 292(8):3172–3185.

Jean, L., Brimijoin, S., and Vaux, D. J. (2019). In vivo localization of human acetylcholinesterase-derived species in a β-sheet conformation at the core of senile plaques in alzheimer's disease. *Journal of Biological Chemistry*, 294(16):6253–6272.

Karr, J. W. and Szalai, V. A. (2007). Role of aspartate-1 in cu (ii) binding to the amyloid-β peptide of alzheimer's disease. *Journal of the American Chemical Society*, 129(13):3796–3797.

Kowalik-Jankowska, T., Ruta, M., Wiśniewska, K., and Łankiewicz, L. (2003). Coordination abilities of the 1–16 and 1–28 fragments of β-amyloid peptide towards copper (ii) ions: a combined potentiometric and spectroscopic study. *Journal of Inorganic Biochemistry*, 95(4):270–282.

Lannfelt, L., Blennow, K., Zetterberg, H., Batsman, S., Ames, D., Harrison, J., Masters, C. L., Targum, S., Bush, A. I., Murdoch, R., et al. (2008). Safety, efficacy, and biomarker findings of pbt2 in targeting aβ as a modifying therapy for alzheimer's disease: a phase iia, double-blind, randomised, placebo-controlled trial. *The Lancet Neurology*, 7(9):779–786.

Lee, M., Kim, J. I., Na, S., and Eom, K. (2018). Metal ions affect the formation and stability of amyloid β aggregates at multiple length scales. *Physical Chemistry Chemical Physics*, 20(13):8951–8961.

Lesné, S., Koh, M. T., Kotilinek, L., Kayed, R., Glabe, C. G., Yang, A., Gallagher, M., and Ashe, K. H. (2006). A specific amyloid-β protein assembly in the brain impairs memory. *Nature*, 440(7082):352.

Mantsyzov, A. B., Savelyev, O. Y., Ivantcova, P. M., Bräse, S., Kudryavtsev, K. V., and Polshakov, V. I. (2018). Theoretical and nmr conformational studies of β-proline oligopeptides with alternating chirality of pyrrolidine units. *Frontiers in Chemistry*, 6:91.

Marino, T., Russo, N., Toscano, M., and Pavelka, M. (2010). On the metal ion (zn 2+, cu 2+) coordination with beta-amyloid peptide: Dft computational study. *Interdisciplinary Sciences: Computational Life Sciences*, 2(1):57–69.

Minicozzi, V., Morante, S., Rossi, G., Stellato, F., Christian, N., and Jansen, K. (2008a). The role of metals in amyloid aggregation—experiments and ab initio simulations. *International Journal of Quantum Chemistry*, 108(11):1992–2015.

Minicozzi, V., Stellato, F., Comai, M., Dalla Serra, M., Potrich, C., Meyer-Klaucke, W., and Morante, S. (2008b). Identifying the minimal copper-and zinc-binding site sequence in amyloid-β peptides. *Journal of Biological Chemistry*, 283(16):10784–10792.

Molina-Sanchez, A. and Wirtz, L. (2011). Phonons in single-layer and few-layer mos 2 and ws 2. *Physical Review B*, 84(15):155413.

Mujika, J. I., Pedregal, J. R.-G., Lopez, X., Ugalde, J. M., Rodríguez-Santiago, L., Sodupe, M., and Maréchal, J.-D. (2017). Elucidating the 3d structures of al (iii)–aβ complexes: a template free strategy based on the pre-organization hypothesis. *Chemical Science*, 8(7):5041–5049.

Mutter, S. T., Deeth, R. J., Turner, M., and Platts, J. A. (2018). Benchmarking of copper (ii) lfmm parameters for studying amyloid-β peptides. *Journal of Biomolecular Structure and Dynamics*, 36(5):1145–1153.

Pappolla, M., Bozner, P., Soto, C., Shao, H., Robakis, N. K., Zagorski, M., Frangione, B., and Ghiso, J. (1998). Inhibition of alzheimer β-fibrillogenesis by melatonin. *Journal of Biological Chemistry*, 273(13):7185–7188.

Perdew, J. P., Burke, K., and Ernzerhof, M. (1996). Generalized gradient approximation made simple. *Physical review letters*, 77(18):3865.

Pflugradt, P., Matthes, L., and Bechstedt, F. (2014). Silicene on metal and metallized surfaces: ab initio studies. *New Journal of Physics*, 16(7):075004.

Rana, M. and Sharma, A. K. (2019). Cu and zn interactions with aβ peptides: Consequence of coordination on aggregation and formation of neurotoxic soluble aβ oligomers. *Metallomics*, 11(1):64–84.

Rauk, A. (2009). The chemistry of alzheimer's disease. *Chemical Society Reviews*, 38(9):2698–2715.

Riley, K. P., Snowdon, D. A., and Markesbery, W. R. (2002). Alzheimer's neurofibrillary pathology and the spectrum of cognitive function: findings from the nun study. *Annals of Neurology*, 51(5):567–577.

Rimola, A., Alí-Torres, J., Rodríguez-Rodríguez, C., Poater, J., Matito, E., Sola, M., and Sodupe, M. (2011). Ab initio design of chelating ligands relevant to alzheimer's disease: Influence of metalloaromaticity. *The Journal of Physical Chemistry A*, 115(45):12659–12666.

Sadigh-Eteghad, S., Sabermarouf, B., Majdi, A., Talebi, M., Farhoudi, M., and Mahmoudi, J. (2015). Amyloid-beta: a crucial factor in alzheimer's disease. *Medical Principles and Practice*, 24(1):1–10.

Šimić, G., Babić Leko, M., Wray, S., Harrington, C., Delalle, I., Jovanov-Milošević, N., Bažadona, D., Buée, L., De Silva, R., Di Giovanni, G., et al. (2016). Tau protein hyperphosphorylation and aggregation in alzheimer's disease and other tauopathies, and possible neuroprotective strategies. *Biomolecules*, 6(1):6.

Streltsov, V. A., Titmuss, S. J., Epa, V. C., Barnham, K. J., Masters, C. L., and Varghese, J. N. (2008). The structure of the amyloid-β peptide high-affinity copper ii binding site in alzheimer disease. *Biophysical Journal*, 95(7):3447–3456.

Strodel, B. and Coskuner-Weber, O. (2019). Transition metal ion interactions with disordered amyloid-β peptides in the pathogenesis of alzheimer's disease: Insights from computational chemistry studies. *Journal of Chemical Information and Modeling*, 59(5):1782–1805.

Syme, C. D., Nadal, R. C., Rigby, S. E., and Viles, J. H. (2004). Copper binding to the amyloid-β (aβ) peptide associated with alzheimer's disease folding, coordination geometry, ph dependence, stoichiometry, and affinity of aβ-(1–28): Insights from a range of complementary spectroscopic techniques. *Journal of Biological Chemistry*, 279(18):18169–18177.

Tõugu, V., Tiiman, A., and Palumaa, P. (2011). Interactions of zn (ii) and cu (ii) ions with alzheimer's amyloid-beta peptide. metal ion binding, contribution to fibrillization and toxicity. *Metallomics*, 3(3):250–261.

Viles, J. H. (2012). Metal ions and amyloid fiber formation in neurodegenerative diseases. copper, zinc and iron in alzheimer's, parkinson's and prion diseases. *Coordination Chemistry Reviews*, 256(19-20):2271–2284.

Wang, J., Ma, F., and Sun, M. (2017). Graphene, hexagonal boron nitride, and their heterostructures: properties and applications. *RSC Advances*, 7(27):16801–16822.

Zhang, Y., Li, P., Feng, J., and Wu, M. (2016). Dysfunction of nmda receptors in alzheimer's disease. *Neurological Sciences*, 37(7):1039–1047.